Electronic Supplementary Information

Synthetic approach for the control of self-doping in luminescent organic semiconductor

Anatoly D. Kuimov, Christina S. Becker, Nikita A. Shumilov, Igor P. Koskin, Alina A. Sonina, Vladislav Yu. Komarov, Inna K. Shundrina, and Maxim S. Kazantsev

1. Characterization

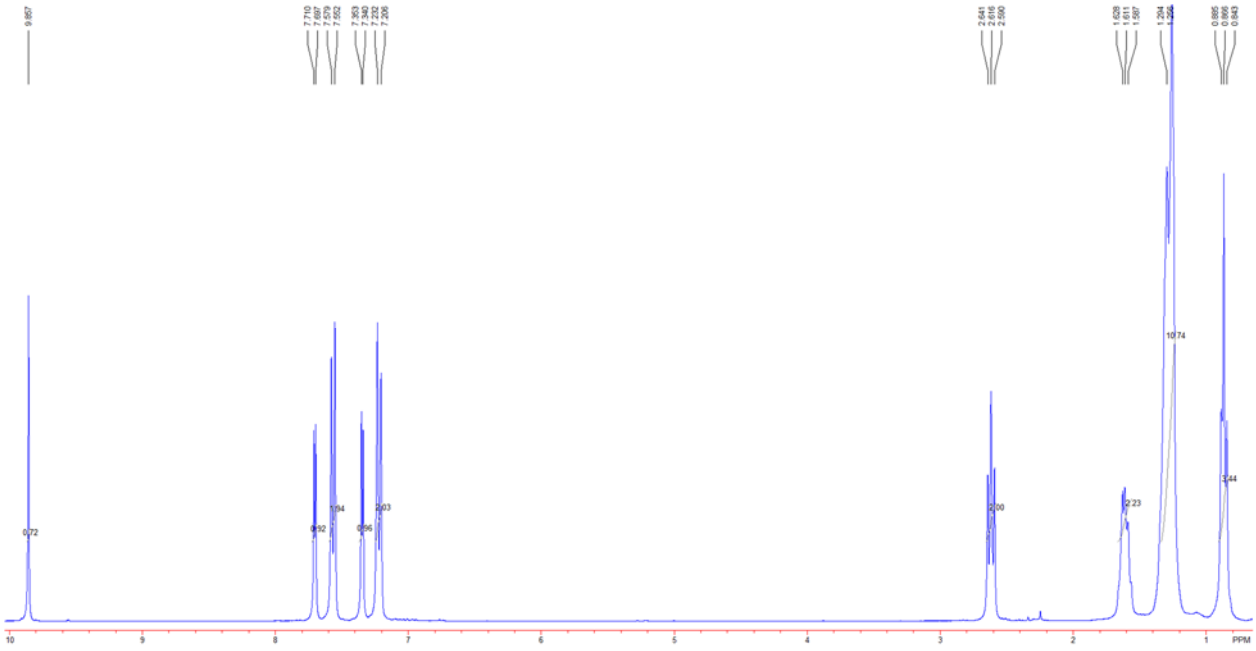

Figure S1. ^{1}H NMR spectrum of compound **3** in $CDCl_3$.

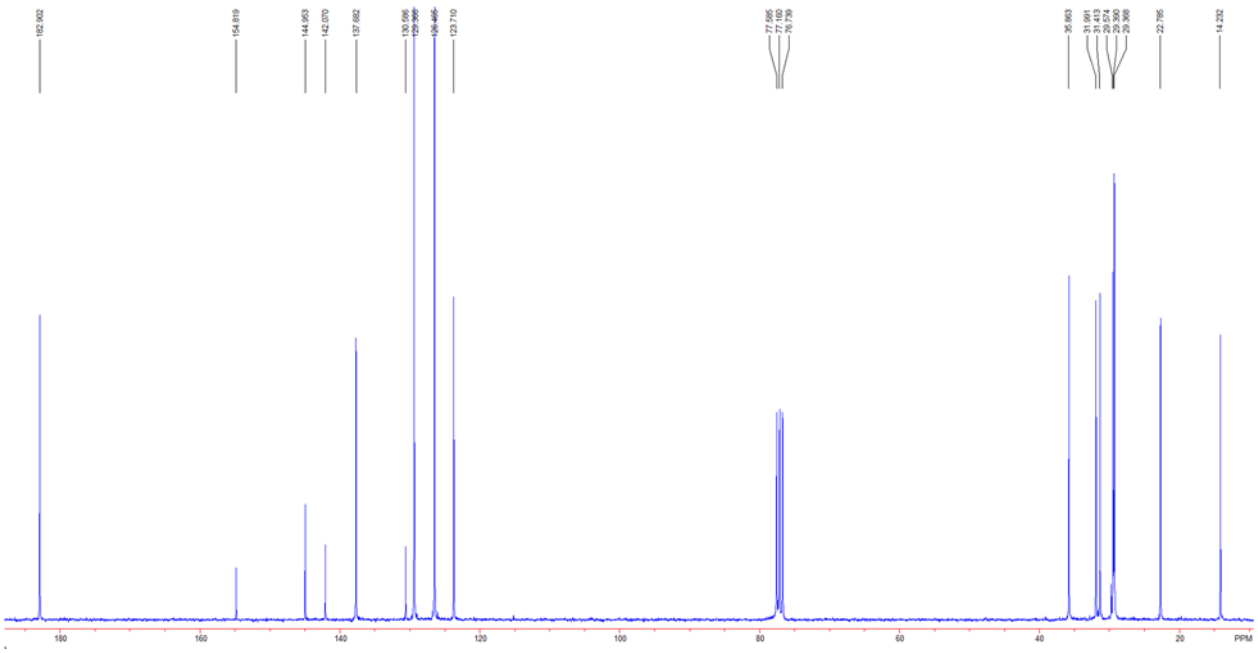

Figure S2. ^{13}C NMR spectrum of compound **3** in $CDCl_3$.

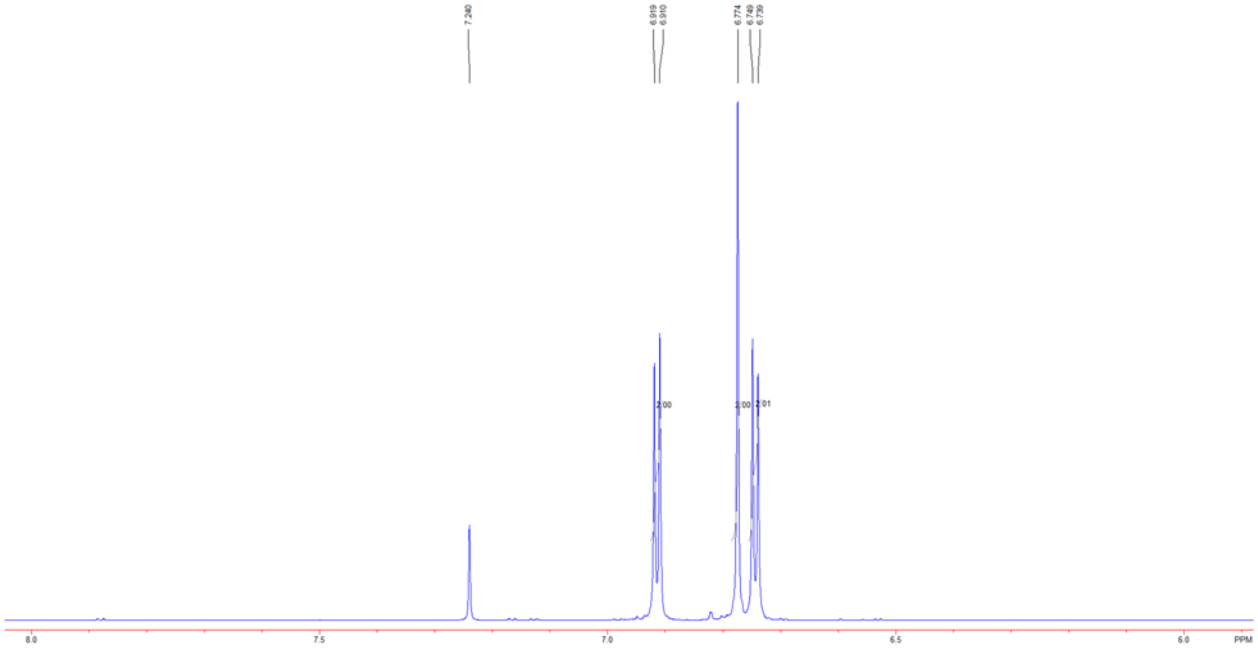

Figure S3. ^{1}H NMR spectrum of compound **6** in $CDCl_3$**.**

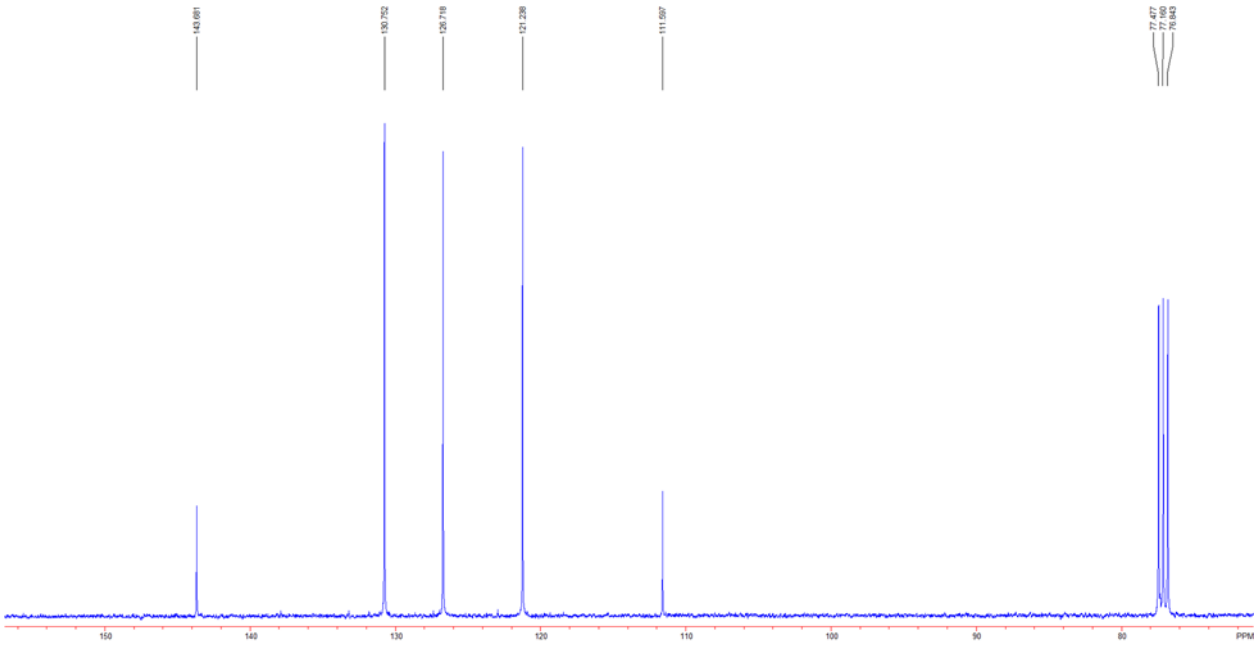

Figure S4. ^{13}C NMR spectrum of compound **6** in $CDCl_3$**.**

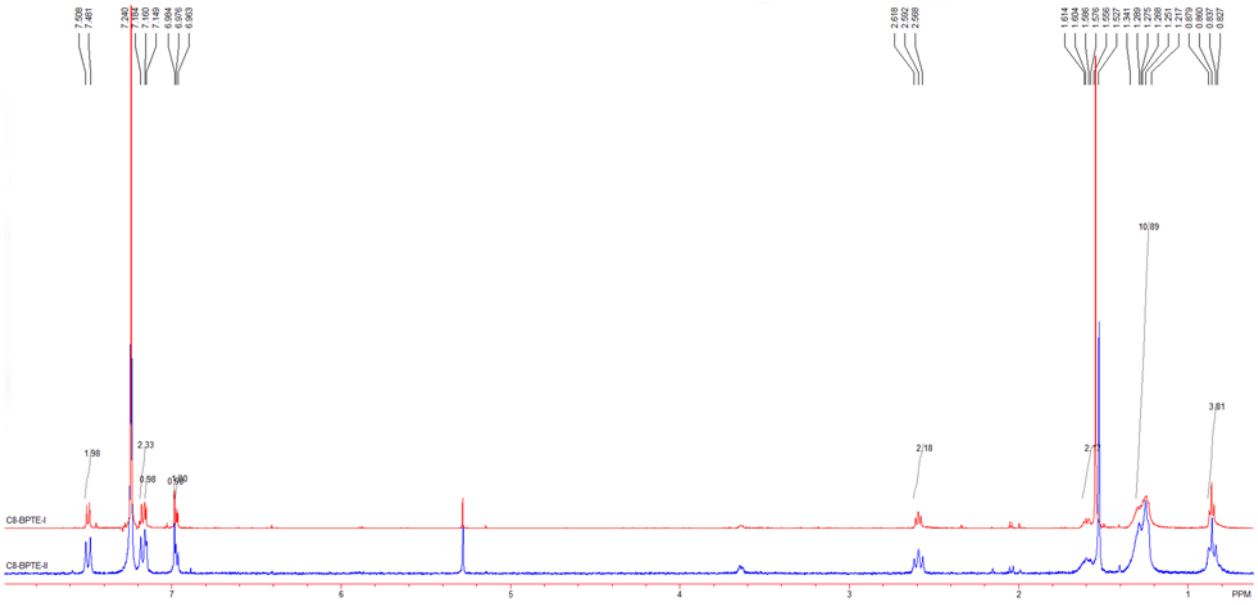

Figure S5. ^{1}H NMR spectra of compounds **C8-BPTE-I** (red) and **C8-BPTE-II** (blue) in $CDCl_3$.

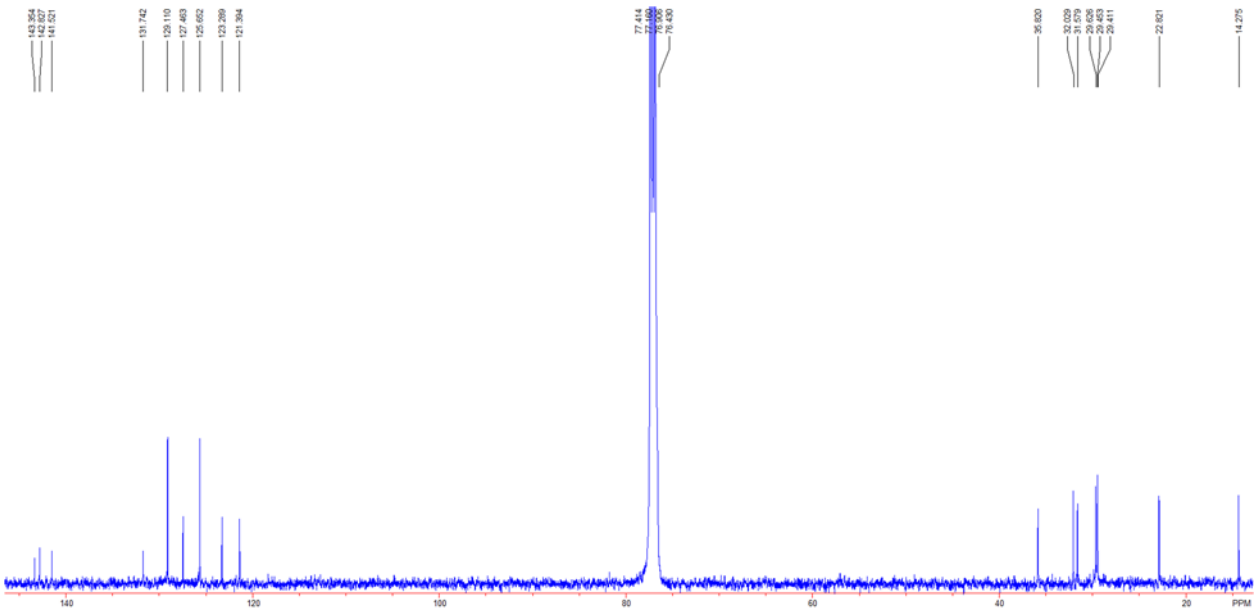

Figure S6. ^{13}C NMR spectrum of compound **C8-BPTE** (batch I) in $CDCl_3$.

Figure S7. IR spectra of compounds C8-BPTE-I (red) and C8-BPTE-II (blue) in KBr pellets.

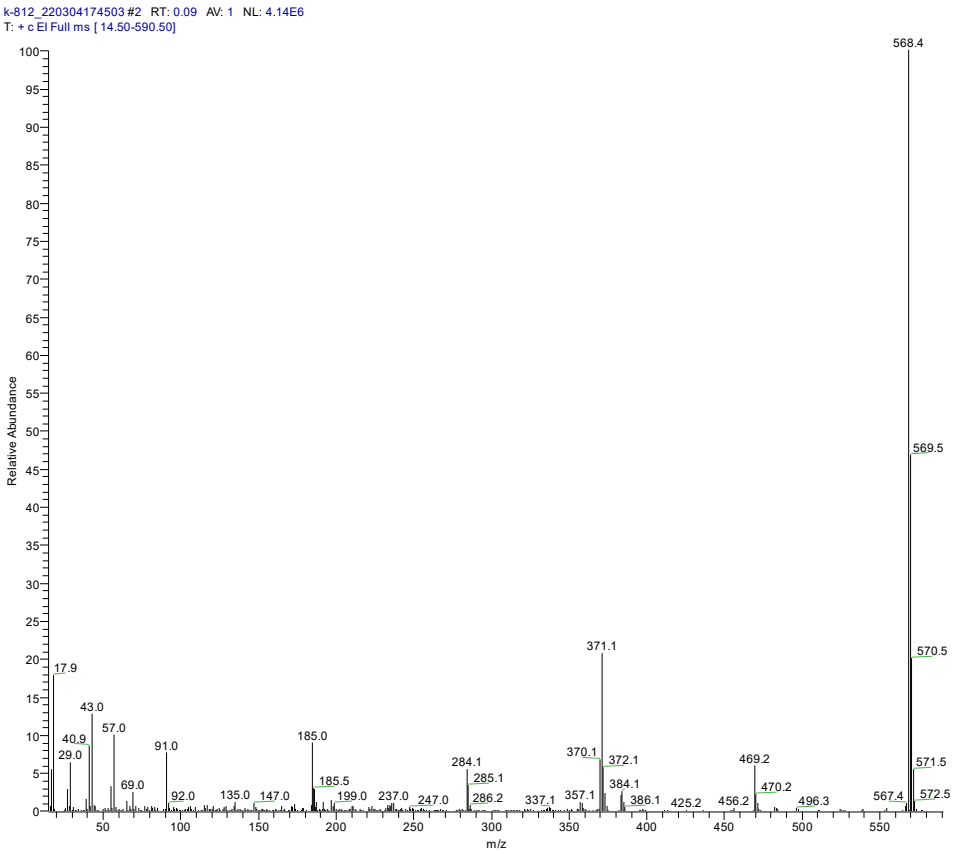

Figure S8. HRMS spectrum of compound C8-BPTE (batch I).

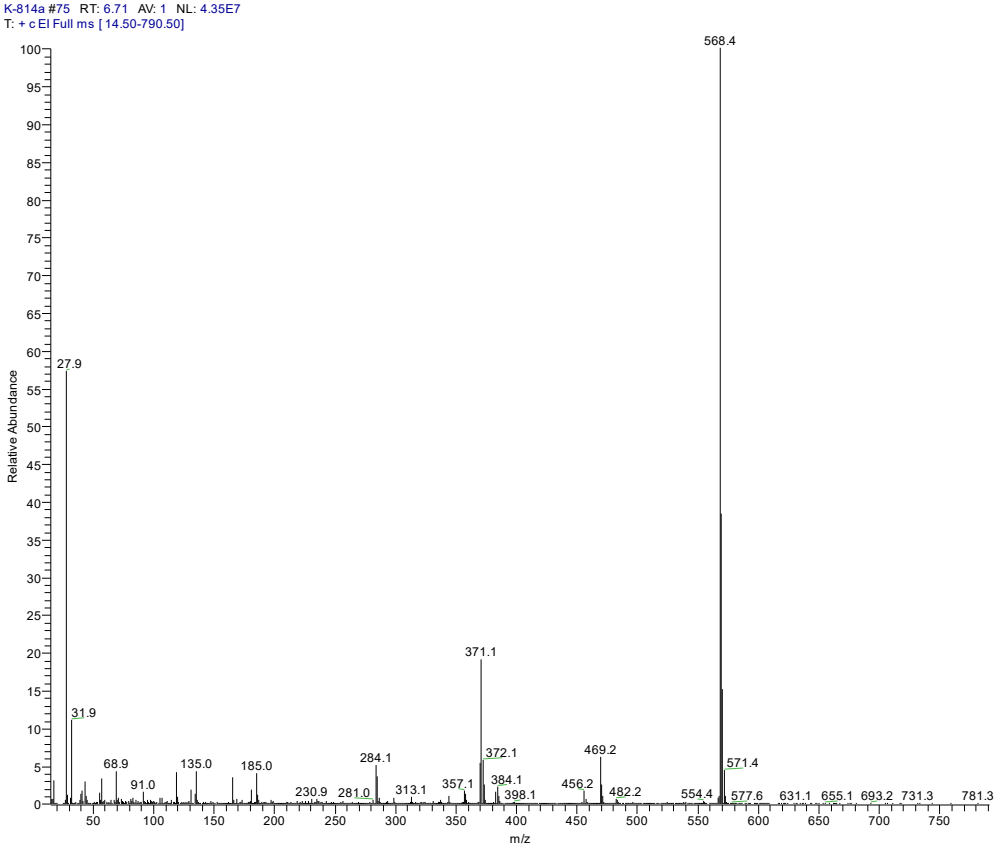

Figure S9. HRMS spectrum of compound C8-BPTE (batch II, full scale). Note that high mass region along with C8-BPTET signal (Figure S10) contains minor peaks 781, 731, 693, 655, 631 and some others which may be assigned to the ions of standard used for MS (perfluorokerosene).

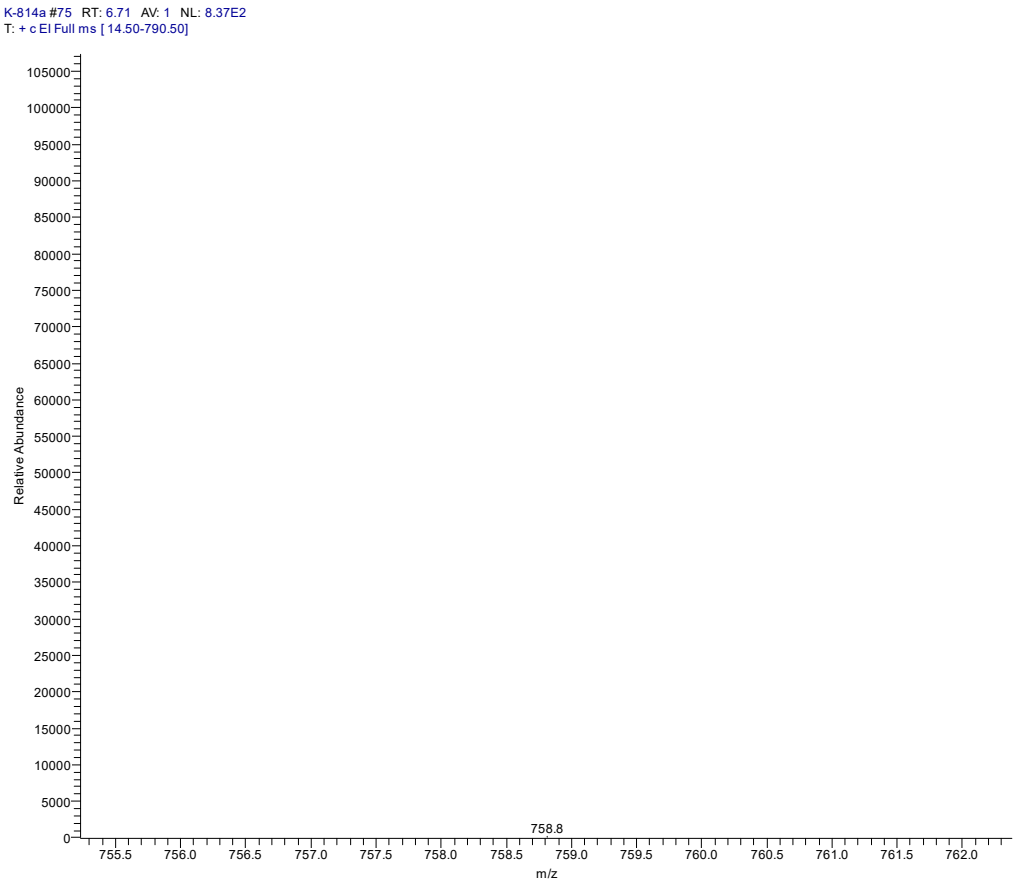

Figure S10. HRMS spectrum of compound C8-BPTE (batch II, zoom of high-mass region).

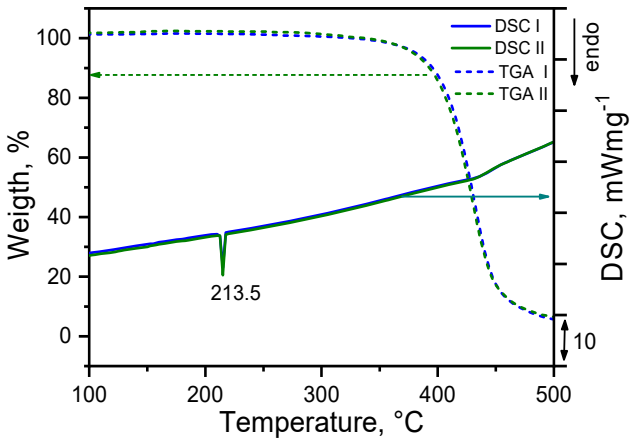

Figure S11. Thermal gravimetric and differential scanning calorimetry analyses of C8-BPTE batch I (blue) and batch II (olive) in He atmosphere.

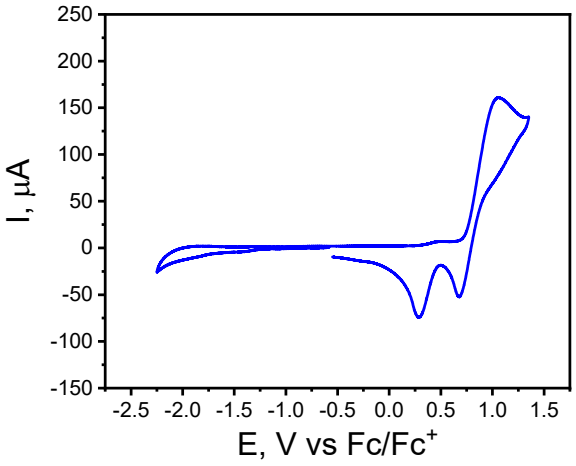

Figure S12. Cyclic voltammogram of C8-BPTE (batch I) in CH_2Cl_2 solution.

2. Quantum chemistry calculations

Table S1. Energy of HOMO (in eV) calculated for optimized geometry of Me-BPTE in gas phase utilizing various DFT functionals and basis sets. Percentage value in the parenthesis represents relative discrepancy between calculated and experimentally estimated value of HOMO energy.

Functional\Basis	6-31+G*	6-311++G**	Def2-TZVP
B3LYP[GD3BJ]	-5.08 (8.3%)	-5.14 (7.2%)	-5.09 (8.1%)
M06-2X	-6.29 (-13.5%)	-6.34 (-14.4%)	-6.29 (-13.5%)
ωB97-X[D]	-6.89 (-24.4%)	-6.97 (-25.8%)	-6.92 (-24.9%)

Table S2. Energy of electron gap (in eV) calculated for optimized geometry of Me-BPTE in the gas phase utilizing various DFT functionals and basis sets. Percentage value in the parenthesis represents relative discrepancy between calculated and experimentally measured value of electron gap.

Functional\Basis	6-31+G*	6-311++G**	Def2-TZVP
B3LYP[GD3BJ]	2.96 (4.6%)	2.99 (5.6%)	3.01 (6.4%)
M06-2X	5.03 (77.7%)	5.06 (78.8%)	5.08 (79.5%)
ωB97-X[D]	6.59 (132.9%)	6.62 (133.9%)	6.63 (134.3%)

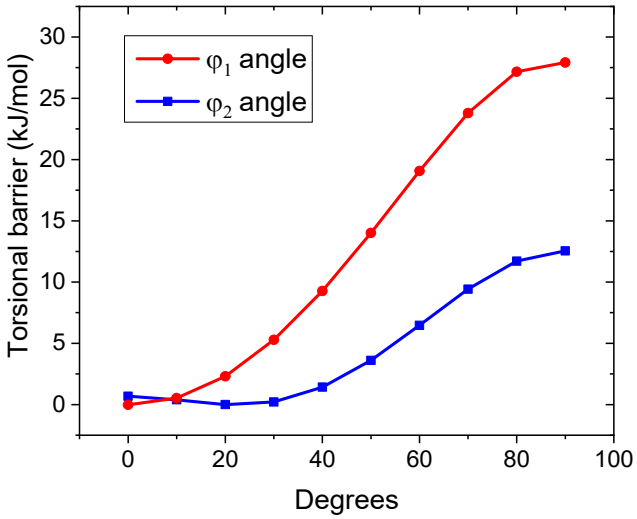

Figure S13. Relaxed potentional energy surface of Me-BPTE upon rotation around φ_1 (blue line and squares) and φ_2 (red line and circles) dihedral angles.

Table S3. Absorption energy of $S_0 \rightarrow S_{1v}$ transition (in nm) calculated for Me-BPTE utilizing various TD-DFT functionals and basis sets. Percentage value in the parenthesis represents relative discrepancy between calculated and experimentally measured value of absorption energy.

Functional\Basis	Def2-TZVP	6-31+G*	6-311++G**
PBE0	430 (4.9%)	429 (4.6%)	431 (5.1%)
B3LYP	443 (7.7%)	443 (7.6%)	445 (8.0%)
CAM-B3LYP	397 (-3.0%)	395 (-3.4%)	398 (-2.9%)
LC-ωPBE	364 (-12.3%)	361 (-13.2%)	363 (-12.6%)
M05	432 (5.4%)	433 (5.5%)	434 (5.7%)
TPSSh	452 (9.6%)	452 (9.5%)	454 (9.8%)
X3LYP	440 (7.1%)	440 (7.1%)	442 (7.5%)

Table S4. Emission energy of $S_{1r} \rightarrow S_0$ transition (in nm) calculated for Me-BPTE utilizing various TD-DFT functionals and basis sets. Percentage value in the parenthesis represents relative discrepancy between calculated and experimentally measured value of emission energy (brightest emission band).

Functional\Basis	6-31+G*	6-311++G**	Def2-TZVP
B3LYP	649 (-25.1%)	652 (-25.4%)	654 (-25.6%)
CAM-B3LYP	582 (-16.6%)	586 (-17.1%)	586 (-17.0%)
PBE0	513 (-5.3%)	516 (-5.8%)	514 (-5.5%)
LC-ωPBE	497 (-2.2%)	501 (-3.0%)	499 (-2.6%)

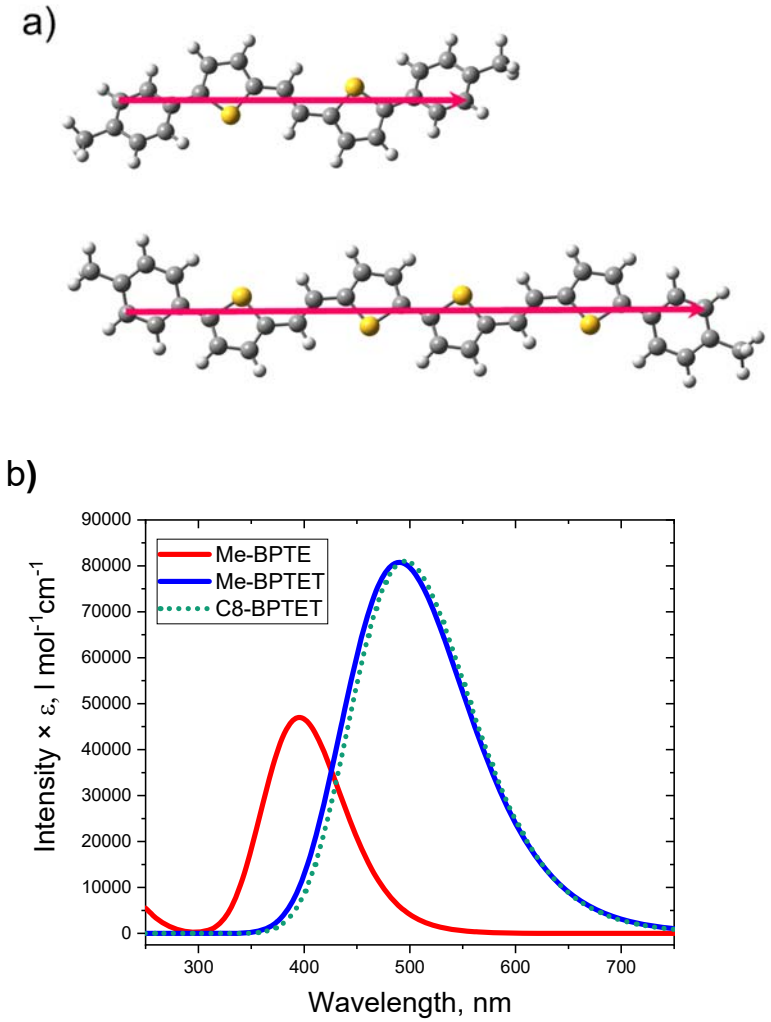

Figure S14. (a) Transition dipole moment (red arrow) of Me-BPTE and Me-BPTET depicted ontop of optimized molecular structure; (b) convoluted optical absorption spectra of Me-BPTE (red line), Me-BPTET (blue line) and C8-BPTET (green dotted line).

3. X-ray data

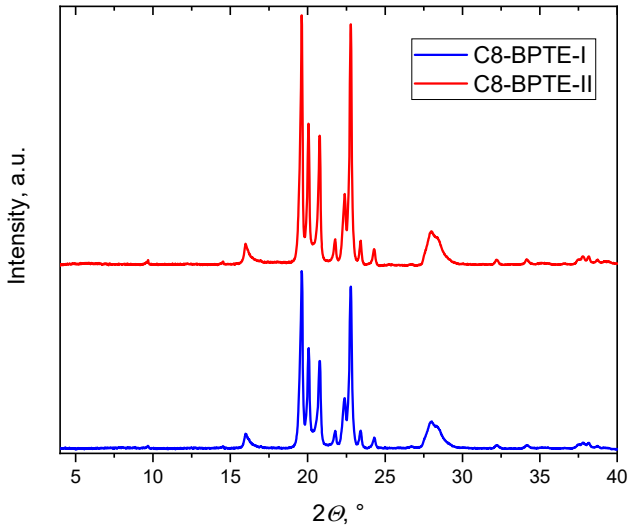

Figure S15. Powder X-ray diffraction patterns of C8-BPTE at ambient temperature.

Table S5. Crystallographic, structural data and experimental details for (E)-1,2-bis(5-bromothiophen-2-yl)ethene and C8-BPTE.

Compound	(E)-1,2-bis(5-bromothiophen-2-yl)ethene		C8-BPTE
Empirical formula	$C_{10}H_6Br_2S_2$		$C_{76}H_{92}S$
Molecular weight	350.09		568.88
Crystal system, space group	Monoclinic, $P2_1/c$		Monoclinic, $C2/m$
Temperature, K	80(3)	299	80(3)
Deposition number	20220319	2166501	20220401
a, *b*, *c* (Å)	13.1360(7), 5.9520(3), 7.3714(4)	13.186 (3), 6.0106 (11), 7.5450 (15)	7.9829(13), 5.3716(10), 35.817(6)
β (°)	102.414(2)	102.762 (5)	92.535(6)
Volume (Å^3)	562.86(5)	583.23 (19)	1534.4(5)
Z	2	2	2
$D_{calcd.}$ (g·cm^{-3})	2.066	1.994	1.231
μ (mm^{-1})	7.53	7.26	0.20
Crystal size (mm)	0.14 × 0.09 × 0.05	0.66 × 0.36 × 0.16	0.27 × 0.14 × 0.005
No. of measured, independent and	7682, 2140, 2008	4186, 1105, 945	8325, 1524, 1359

observed [$I > 2\sigma(I)$] reflections			
R_{int}	0.026	0.051	0.056
Range of h, k, l	$-20 \le h \le 17$, $-9 \le k \le 9$, $-10 \le l \le 11$	$-16 \le h \le 16$, $-6 \le k \le 7$, $-9 \le l \le 9$	$-9 \le h \le 9$, $-6 \le k \le 6$, $-42 \le l \le 42$
$R[F^2 > 2\sigma(F^2)]$, $wR(F^2)$, S	0.016, 0.040, 1.09	0.027, 0.072, 1.05	0.121, 0.394, 1.26
No. of parameters	64	64	147
No. of restraints	0	0	167
$\Delta\rho_{max}$, $\Delta\rho_{min}$ (e Å^{-3})	0.44/-0.39	0.30/-0.63	0.56/-0.75

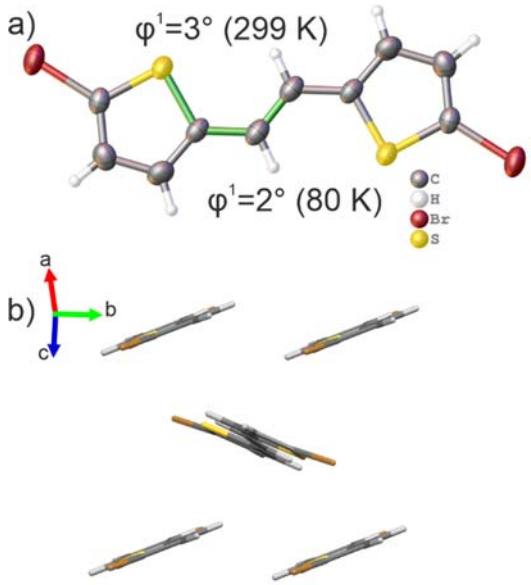

Figure S16. Molecular structure with torsional angle φ^1 at 299 K and 80 K (a) and fragment of crystal structure (b) of (E)-1,2-bis(5-bromothiophen-2-yl)ethene. The arrows indicate the orientation of crystallographic axes.

4. OFET Data

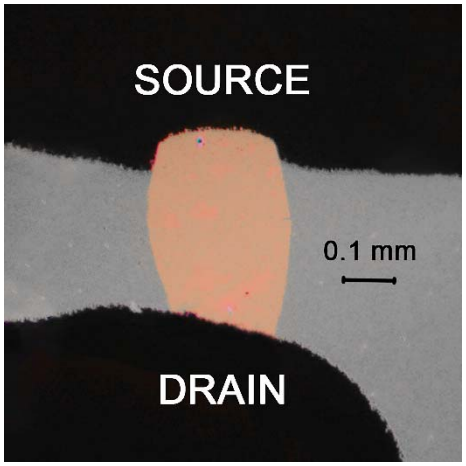

Figure S17. Optical image of C8-BPTE OFET.

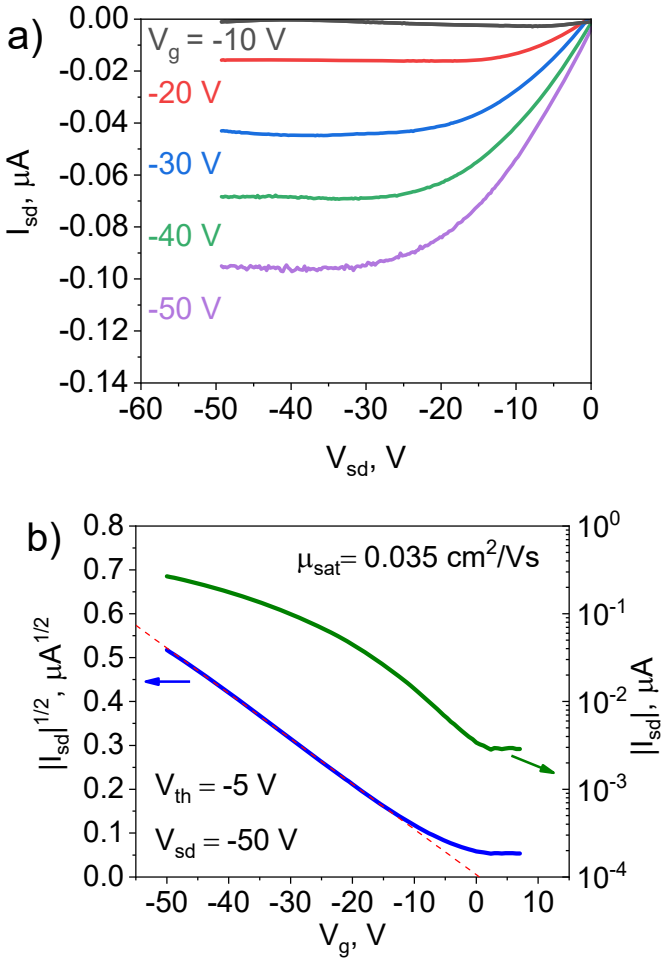

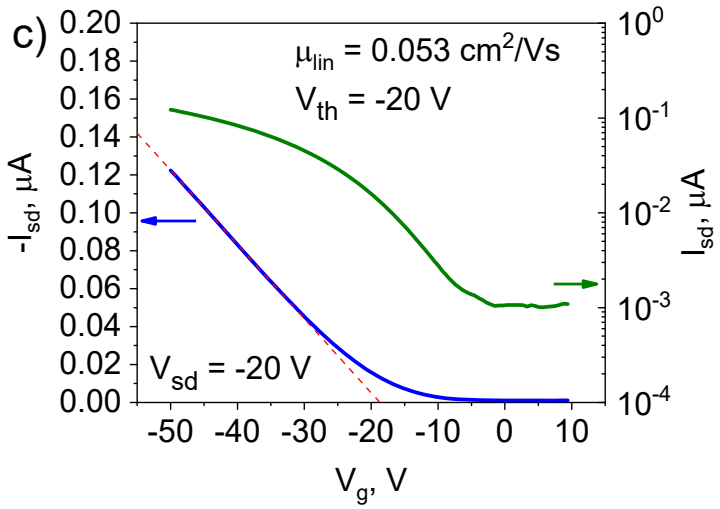

Figure S18. Output (a) and transfer characteristics in saturation (b) and linear (c) regimes of C8-BPTE (batch II) single crystal OFET.

Table S6. Charge transport parameters of C8-BPTE (Batch I and Batch II) OFETs.

	Sample	W/L	μ_{sat}, cm^2/Vs	V^{th}_{sat}, V	μ_{lin}, cm^2/Vs	V^{th}_{lin}, V
Batch I	1.	0.87	0.059	0	0.033	-28
	2.	0.95	0.08	-4	0.067	-21
	3.	0.62	0.051	-3	0.053	-20
	4.	0.87	0.021	0	0.019	-20
	5.	1.1	0.031	-8	0.032	-29
	6.	1	0.073	-3	0.063	-31
	7.	1.07	0.023	-7	0.019	-20
	8.	0.81	0.029	-3	0.028	-19
	9.	0.82	0.053	-6	0.048	-18
	10.	4.29	0.029	4	0.032	-17
	11.	1.51	0.095	15	0.089	0
	12.	0.61	0.078	-12	0.085	-23
	13.	1.97	0.044	24	0.041	-7
	14.	0.45	0.094	16	0.097	-4
	15.	0.77	0.032	-10	0.023	-18

	16.	0.59	0.1	-6	0.087	-17
	17.	0.37	0.096	-2	0.08	-12
	Average		0.058 ± 0.028	-0.3±9.8	0.053±0.027	-17.9 ± 8.4
Batch II	1.	0.7	0.035	-5	0.032	-20
	2.	0.53	0.021	-6	0.019	-20
	3.	0.78	0.057	-19	0.056	-31
	4.	0.31	0.058	-4	0.058	-24
	5.	0.6	0.039	-6	0.031	-26
	6.	1.22	0.023	-12	0.021	-31
	7.	1.75	0.034	-14	0.019	-29
	8.	1.18	0.028	-9	0.02	-21
	9.	0.52	0.029	-4	0.024	-25
	Average		0.036 ± 0.013	-10.1 ± 5.4	0.031 ± 0.015	-25.2 ± 4.4

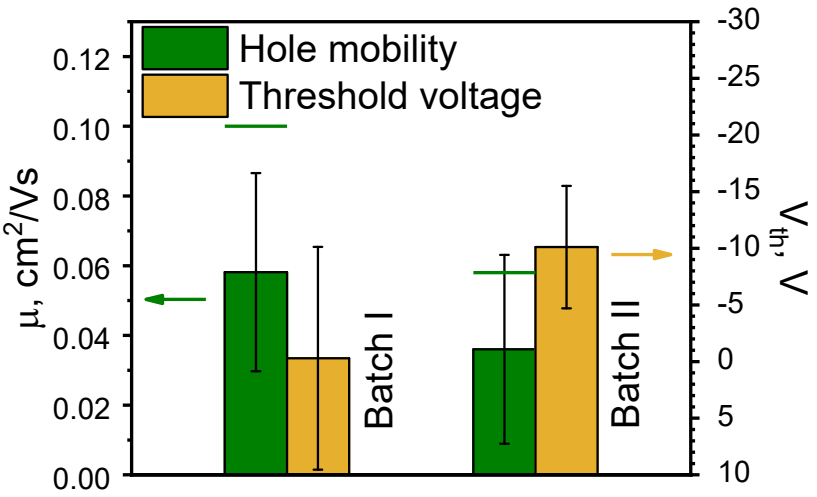

Figure S19. Average hole mobility and threshold voltage in saturation regime of C8-BPTE OFETs (Batch I and Batch II); the horizontal marks indicate the maximal values.